Ion implantation for figure correction of thin X-ray telescope mirror substrates

Brandon Chalifoux*[a], Graham Wright[b], Ralf K. Heilmann[c], Mark L. Schattenburg[c]
[a]Dept. of Mechanical Engineering, MIT, Cambridge, MA, USA 02139
[b]Plasma Science and Fusion Center, MIT, Cambridge, MA, USA 02139
[c]Space Nanotechnology Lab, MIT Kavli Institute, Cambridge, MA, USA 02139
*bchal@mit.edu; phone: (860) 377-1570; fax: (617) 452-2888; snl.mit.edu

ABSTRACT

Figure correction of X-ray telescope mirrors will be critical for future missions that require high angular resolution and large collecting areas. In this paper, we show that ion implantation offers a method of correcting figure errors by imparting sub-surface in-plane stress in a controllable magnitude and location in Schott D-263 glass, Corning Eagle XG glass, and crystalline silicon substrates. In addition, we can in theory achieve nearly exact corrections in Schott D-263 glass, by controlling the *direction* of the stress. We show that sufficient stress may be applied to Schott D-263 glass to achieve figure correction in mirrors with simulated initial figure errors. We also report on progress of a system that will be capable of correcting conical shell mirror substrates.

Keywords: X-ray mirrors, figure correction, plane stress, mismatch strain, ion implantation, glass, silicon

1. INTRODUCTION

The next X-ray observatory will require extremely accurate mirror substrates in order to achieve the stated goal of 0.5 arcsecond half-power diameter (HPD) angular resolution with 30 times greater effective area than the Chandra X-ray Observatory[1]. One potential route to fabricating sufficiently accurate mirrors is to first make a substrate with decent figure, small mid-spatial frequency errors, and low micro-roughness; and to correct the figure error by generating in-plane stress to impose a controlled distortion in the substrate. Ion implantation, illustrated in Figure 1, is a viable method of generating this in-plane stress. Ion implantation also enables, at least in Schott D-263 glass, a near-exact figure correction, in a kinematically-mounted mirror, by controlling the *direction* of stress in addition to the location and magnitude. In addition, the time required to implant enough ions could be on the order of a few hours per mirror with a research accelerator, and much faster with a commercial accelerator.

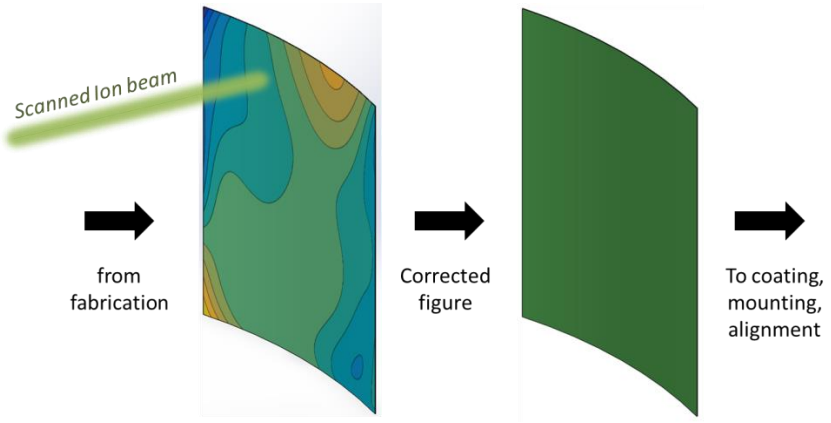

Figure 1. Substrates may be corrected by raster-scanning an ion beam, dwelling longer for higher stress.

Slumped glass[2,3,4] or crystalline silicon[5] may be viable substrate materials. To date, the best mirror substrates have been made with Schott D-263 glass by NASA Goddard Space Flight Center[2]. The limitation appears to be mid-frequency ripples, which will be difficult to correct with any stress-based figure correction scheme, but could possibly be addressed using differential deposition[6]. As such, our group at MIT is developing air bearing slumping[3], which we expect to produce acceptable figure with minimal mid-frequency ripples.

Several methods of figure correction are being evaluated by other groups that rely on applying equi-biaxial stress on mirror substrates in a controllable magnitude and location[7,8]. With any of these methods, to achieve a near-exact correction of thin shell substrates, as would be required for a 0.5 arcsecond telescope, we require the correction scheme to either:

1. apply an **equi-biaxial stress**, and have a stable, over-constrained mounting scheme that provides the necessary reactions to allow a good correction[7]; or
2. apply a **general stress** to achieve a near-perfect correction in a free mirror, and use a mounting scheme that minimizes the disturbance to the mirror

The ability to apply a general stress state, which ion implantation provides, requires lower correction stress and allows the mirrors to be mounted kinematically. We discuss this in Section 2.

In Section 3, we show experimental results demonstrating that substantial *equi-biaxial and uniaxial* stress may be generated in Schott D-263 glass. In other words, a general stress state may be applied in this material, allowing near-exact correction. In addition, we show experimental results for equi-biaxial stress in Corning Eagle XG glass and crystalline silicon. For these two materials, we have not observed substantial uniaxial stress, but the magnitude of measured equi-biaxial stress appears sufficient to match the correction performance of piezo-electric actuators.

It is important to understand what figure errors may be corrected by applying a general stress state, given that the stress that we may apply with ion implantation is limited, as with any other method. In Section 4, we show results from Monte Carlo simulations of fictive surfaces with realistic power spectral density functions. We find that many surfaces may be corrected to better than 0.05 arcsecond HPD, but this becomes more difficult as the radius of curvature decreases. We also performed Monte Carlo simulations to understand how sensitive corrections are to the stress magnitude.

2. THE IMPORTANCE OF CONTROLLING STRESS DIRECTION

At least three groups are currently investigating methods of correcting figure errors in thin X-ray telescope mirror substrates using in-plane stress, as described by O'Dell, et al.[9]. In each of these methods, a strain (known as a mismatch strain) is generated in a thin film on the surface of the mirror substrate. A stress in the film arises from this mismatch strain. The integration of the film stress over the thickness of the film, called the integrated stress, must be balanced by bending in the substrate. All of the methods currently being studied rely on the ability to change the magnitude and location of the mismatch strain (and therefore the stress). However, this is not enough to achieve perfect correction in a free substrate. In order to achieve near-perfect correction, we must control the *direction* of stress in addition to the magnitude and location. We have found that substrates may be corrected, in theory, to a residual RMS slope error of 0.01 arcsecond or better; we will refer to this as a full correction for simplicity, while acknowledging that it has not been proven that this provides a perfect correction.

The film with a mismatch strain is left in a state of plane stress (i.e., the stress components normal to the surface are zero), and there are three non-zero components of stress: two normal stresses, and a shear stress. Other than ion implantation, all stress-based figure correction methods under consideration allow control of the equi-biaxial stress only;

that is, the two normal stress components are equal, and the shear stress is zero. However, as several groups have found, good correction with equi-biaxial stress may be achieved by relying on the mounting structure[10,11], but equi-biaxial stress alone does not appear to be sufficient for full correction.

If we can control the three components of plane stress (which we refer to as general stress control), then we may nearly perfectly correct a mirror substrate, and we may then mount it kinematically. This offers a few advantages compared to an over-constrained mounting scheme. First, the goal of the mount is to distort the mirror as little as possible, which may be easier than requiring the mount to maintain a specified non-zero stress state. Second, a perfectly-kinematic mount would allow only rigid body deformations of the mirror, and not figure distortions. Third, a kinematic mount would be easier to align. The group at NASA Goddard Space Flight Center[12] is currently working on a mounting scheme that is approximately kinematic, and it is expected to provide lower distortion than the current, over-constrained scheme. However, to achieve adequate correction of figure errors in a free mirror, we require general stress control.

2.1 Example in flat plates

The necessity of controlling the different components of the plane stress tensor is simplest to understand by considering a thin flat round plate with a figure error described by a set of Zernike polynomials. For reference, a table of Zernike polynomials (excluding tip, tilt, and piston) is shown in Figure 2. We may impose a mismatch strain between the substrate and a thin film. The equilibrium equations describing this system have been derived by Huang, et al.[13]. With some tedious algebra, we may show that Zernike polynomial mismatch strain fields are solutions to these bi-harmonic governing equations. Since this subject is not the focus of this paper, only some relevant observations will be described.

We note that this mismatch strain results in a stress in the film, which is ultimately what causes deformation. However, any "stress-based figure correction" method actually imposes the mismatch strain. Here, we refer to the mismatch strain fields, but it is equally acceptable to consider stress fields. In Section 3, we report stress magnitudes, not strain.

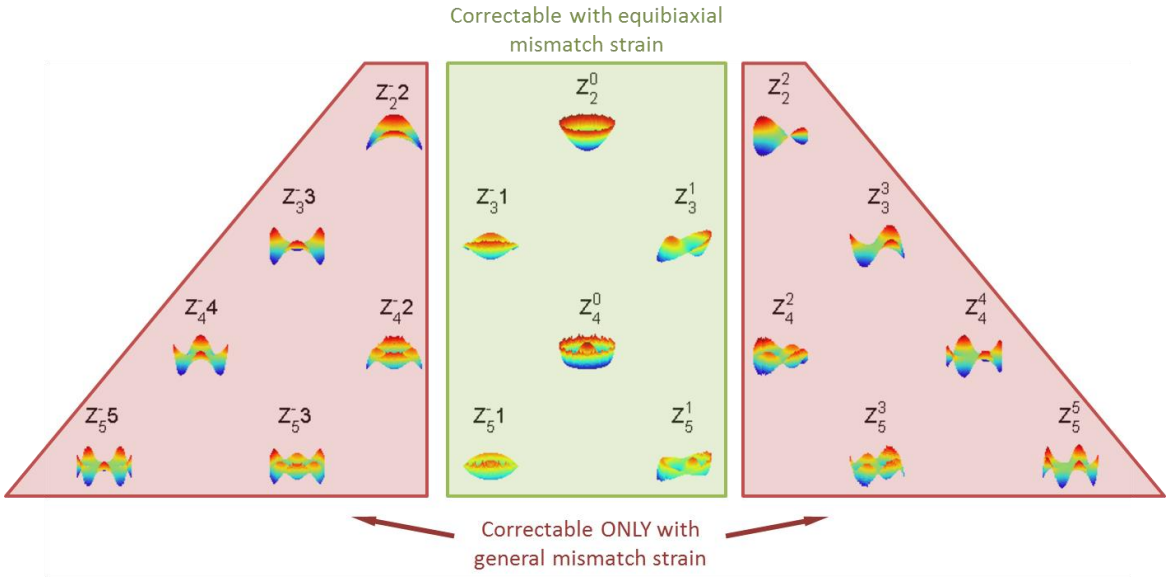

Figure 2. Table of Zernike polynomials illustrating which figure errors may be corrected with equi-biaxial mismatch strain. All shapes may be corrected with a general mismatch strain.

If we consider a flat plate with only spherical figure error, Z_2^0, we may correct this simply by imposing a uniform equi-biaxial mismatch strain on the surface in the proper magnitude. Likewise, any figure error in the central three columns (highlighted in green in Figure 2) may be exactly corrected by imposing equi-biaxial strain on the surface.

In contrast, if we consider a flat plate with only astigmatism error, $Z_2^{\pm 2}$, we find that there is no equi-biaxial strain that exactly corrects this error. In fact, this is the case with all of the Zernike polynomials outside the central three columns (highlighted in red in Figure 2). Any attempt to correct the polynomials outside the central three columns generates new errors at the edge of the pyramid. In order to correct these errors, we require a general mismatch strain.

This problem is exacerbated by the curved substrates used for X-ray telescope mirrors, and becomes more problematic as the radius of curvature is decreased. In order to achieve a correction sufficient for a telescope with a 0.5-arcsecond half-power diameter point-spread function, without imposing external loading via the mirror mounts, we must be able to control different components of the mismatch strain tensor. This is illustrated in Section 2.2.

2.2 Correction of conical shell substrates: a rough comparison

In this section, we consider a particular mirror figure error, shown in Figure 3. We aim to correct this mirror, mounted kinematically, using (1) an equi-biaxial mismatch strain field; and later, (2) a general mismatch strain field. We note that this figure error is pure fantasy and is limited to very low spatial frequencies with the intention of making this as easy to correct as possible; in Section 4, we consider much more realistic surface figure errors than this. The point of this study is simply to illustrate that controlling the components of strain independently results in better correction, at much lower stress magnitude, and with a smooth stress field. More effort in optimizing these methods may result in improvements in both cases, but these results illustrate the comparison.

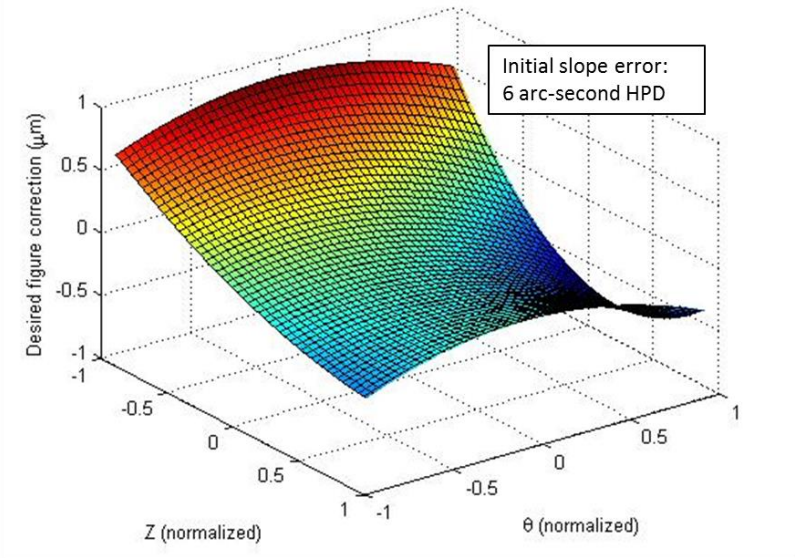

Figure 3. A sample figure error, used to compare effectiveness of equi-biaxial stress and general stress control

We may calculate the equi-biaxial strain field required to correct a given figure error by the following process, described in more detail by Chalifoux[14]. First, we calculate the influence function of a test mismatch strain at each node of a finite element model. We then perform a constrained least squares optimization, using a trust-region-reflective algorithm in MATLAB, of the equi-biaxial mismatch strain magnitudes, with the goal to minimize surface height error (for

computational simplicity). The magnitude of strain is constrained, allowing for implantation on both the front and rear surfaces of the substrate. Once the minimum surface height error is obtained, the residual axial slope error is calculated. Figure 4 shows the results of this process. As expected, the residual error decreases as the limit on integrated stress increases. In addition, for mirrors with a larger radius of curvature, the correction is more complete.

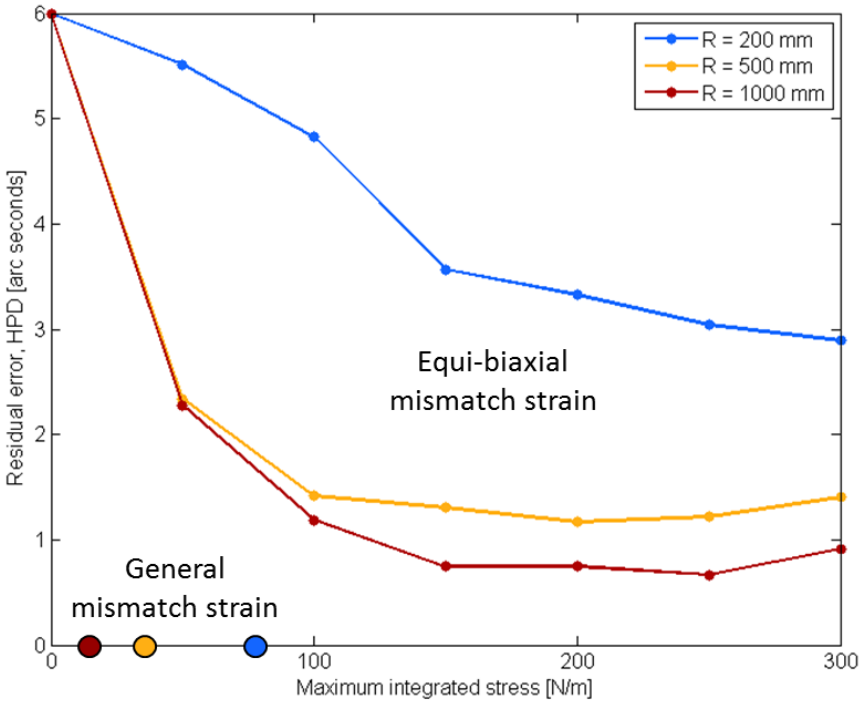

Figure 4. Both the residual error and required stress magnitude are significantly lower for a general strain than for an equi-biaxial strain. Using equi-biaxial strain fields results in a plateau just under 1 arcsecond HPD.

In order to calculate the general mismatch strain field required to correct this same figure error, we may use a simpler procedure. Instead of calculating influence functions at each node, we may impose test mismatch strain fields with magnitudes described by polynomials (in this case, we are using Legendre-Legendre polynomials). We impose one polynomial for an equi-biaxial strain, one for an anti-biaxial strain (where the mismatch normal strain in one direction is opposite in sign but equal in magnitude to the other normal strain), and one for a shear strain (which is equal to an anti-biaxial strain but rotated by 45° on the surface). We may then perform an unconstrained linear least squares fit, using the psuedoinverse of a matrix containing the responses to each test input strain function, to the desired figure correction. We find that the magnitude of stress required is achievable for a full correction, so we do not need to employ constrained optimization when we impose a general mismatch strain field.

In Figure 4, we see that using a general mismatch strain we get excellent correction of each of the mirror substrates, using a much lower magnitude of stress. While this study is not definitive, it is consistent with the findings of Davis, et al.[15], who found that correcting mirrors with equi-biaxial strain and a kinematic mount is not very effective. It is also consistent with the work of Kolodziejczak, et al.[10], who found that figure correction using equi-biaxial strain is more difficult with smaller mirror radii. Neither of these studies, nor the one reported here, shows full correction of mirror substrates when using equi-biaxial mismatch strain only. This is consistent with the observations for flat plates, described in Section 2.1.

3. EXPERIMENTAL STRESS MEASUREMENTS

3.1 Equi-biaxial stress

Implanting ions at normal-incidence to a surface results in equi-biaxial stress through several mechanisms, depending on the ion beam parameters and the substrate material. This equi-biaxial stress, much like piezo-electric actuators or magneto-strictive films, may be used to correct figure errors in conical shell mirror substrates. As we have seen in Section 2, and as shown by Reid, et al.[7], correcting figure errors to a good enough figure for a 0.5 arcsecond telescope, using only equi-biaxial stress, would require a mounting scheme that over-constrains the mirror, but it may be possible.

Figure 5 shows the equi-biaxial stress measured while implanting ions at normal incidence to the sample surface, in Schott D-263 glass and Corning Eagle XG glass. Figure 6 shows equi-biaxial stress in crystalline silicon. Table 1 lists the ion beam parameters for these experiments. These data were obtained using an in-situ curvature measurement device, described by Chalifoux, et al.[16]. It is clear that the different materials exhibit significantly different behavior; the physics behind this are fairly well-understood, and are described in Section 3.3.

To obtain these results in glass, we have used high-energy light ions, for two reasons: (1) the depth of implantation is larger, so the integrated stress may be higher; and (2) a thermal-spike-driven stress generation mechanism (recently reviewed by Klaumünzer[17]) becomes more pronounced in this regime. Indeed, the magnitude of stress generated in Schott D-263 implanted with 6 MeV Si^{+++} ions is about an order of magnitude higher than the stress generated with 0.8 MeV Si^{+} ions, as shown in Figure 7.

The behavior of stress generated by ion implantation into silicon is believed to be dominated by amorphization of crystalline silicon, which causes a compressive stress to build up. We have seen little increase in stress in silicon resulting from high-energy implants, or from implants with light ions. Amorphization is believed to be primarily a result of damage due to nuclear collisions between the ions and substrate atoms[19]. The number of nuclear collisions per ion increases as the ion mass is increased, and as the ion energy is decreased. A significantly higher mirror correction throughput may be achieved using heavy ions at lower energy, where these nuclear collisions become more dominant.

Substrate material	Schott D-263	Schott D-263	Corning Eagle	silicon	Schott D-263
Ion energy [MeV]	0.8	6	6	6	6
Ion species	Si^{+++}	Si^{+++}	Si^{+++}	Si^{+++}	O^{+++}
Angle of incidence [°]	0	0	0	0	45
Ion flux [ion cm^{-2} sec^{-1}]	6 x 10^{10}	2.5 x 10^{10}	1 x 10^{11}	2 x 10^{11}	1.2 x 10^{10}
Max. equi-biaxial integrated stress [N/m]	+30	-250	+250	-100	-50 equibiaxial, +100 uni-axial

Table 1. Experimental parameters for the plots in Section 3.

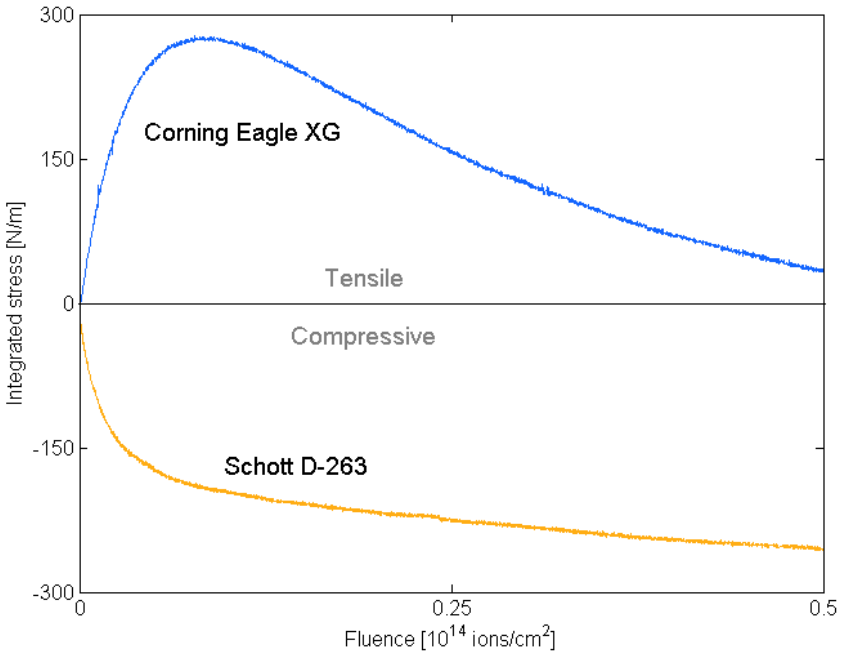

Figure 5. Equi-biaxial integrated stress in Corning Eagle XG and Schott D-263 glass, generated by implanting 6 MeV Si^{+++} ions at normal incidence. The maximum magnitude is about 250 N/m for each.

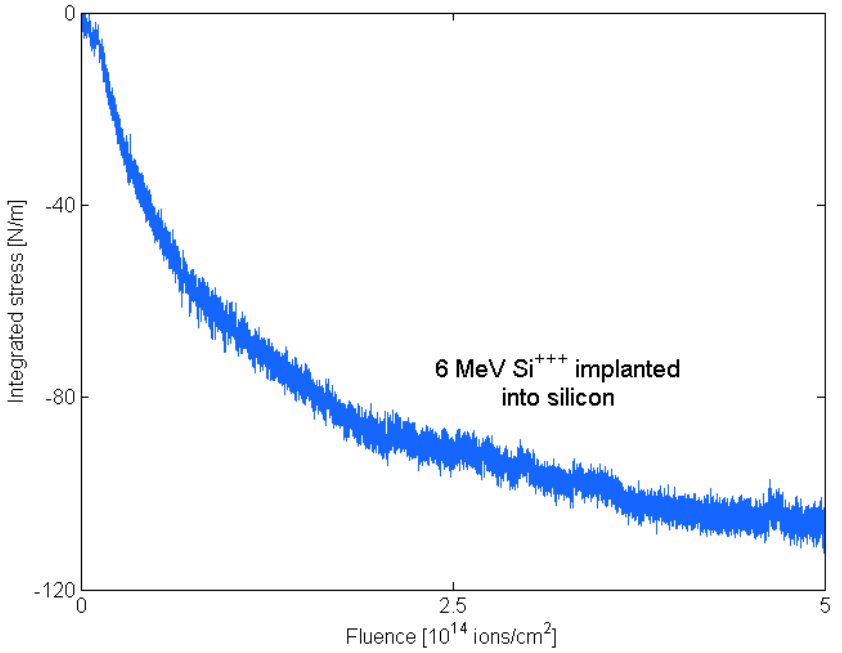

Figure 6. Equi-biaxial integrated stress in crystalline silicon, generated by implanting 6 MeV Si^{+++} ions at normal incidence. The maximum magnitude is 110 N/m.

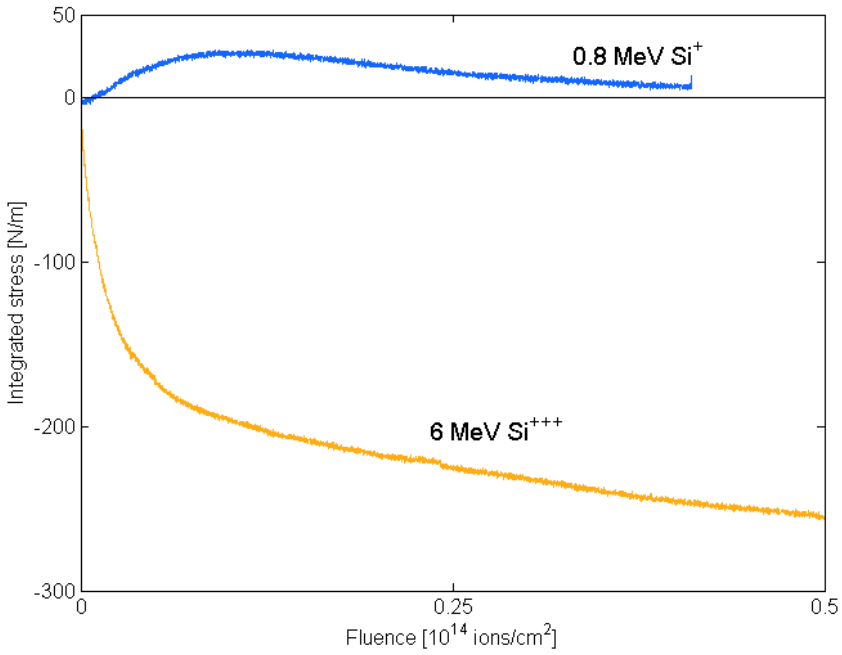

Figure 7. Equi-biaxial integrated stress in D-263 glass is significantly different at different ion energies.

3.2 Uni-axial stress

We have shown, in Section 2, that controlling the magnitude, location, and *direction* of stress are all important for figure correction of conical shell mirror substrates in a kinematic mount. Here, we show experimental results demonstrating that large anisotropic stress is generated from angled implants of high-energy light ions into Schott D-263 glass. We will show in Section 4 that we can correct many initial figure errors using the magnitudes of stress that we measure.

Similar to the experiments with normal-incidence implants, we measured stress with an in-situ curvature measurement device. In this case, the device measures curvature in two directions. All of these experiments were performed at a 45° ion beam angle of incidence. More details may be found in Table 1. Figure 8 shows results for 6 MeV O^{+++} ions implanted into Schott D-263. We measured two stresses: uni-axial, which is along the projection of the ion beam onto the surface; and equi-biaxial. Here, we are able to achieve a uniaxial stress of +100 N/m and an equibiaxial stress of -50 N/m. It is possible that by tuning the ion beam angle of incidence, we may achieve a more pure uniaxial stress.

To understand the choice of stress representation as uni-axial and equi-biaxial stress, consider a general state of plane stress, illustrated by Mohr's circle (refer to Figure 9). This state of stress, shown in blue (1), has three components: two normal stresses and a shear stress. An equivalent state of stress, but expressed in a rotated coordinate frame, is shown in green (2), and consists of only two normal stresses (i.e., the principal stresses). Since our results show a more tensile stress in the beam-parallel direction than in the beam-perpendicular direction, we may express our results in terms of an equi-biaxial stress (the lower principal stress), and a uni-axial stress (the difference between the principal stresses), shown in red (3). This is useful because an angled implant provides a nearly uni-axial stress, while a normal-incidence implant results in equi-biaxial stress.

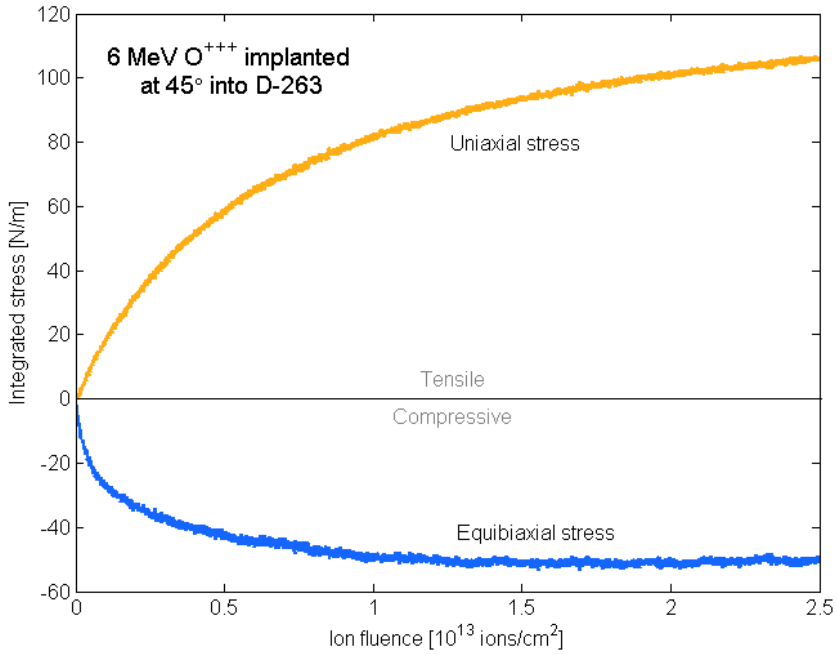

Figure 8. Angled implant into D-263 glass, showing highly anisotropic stress

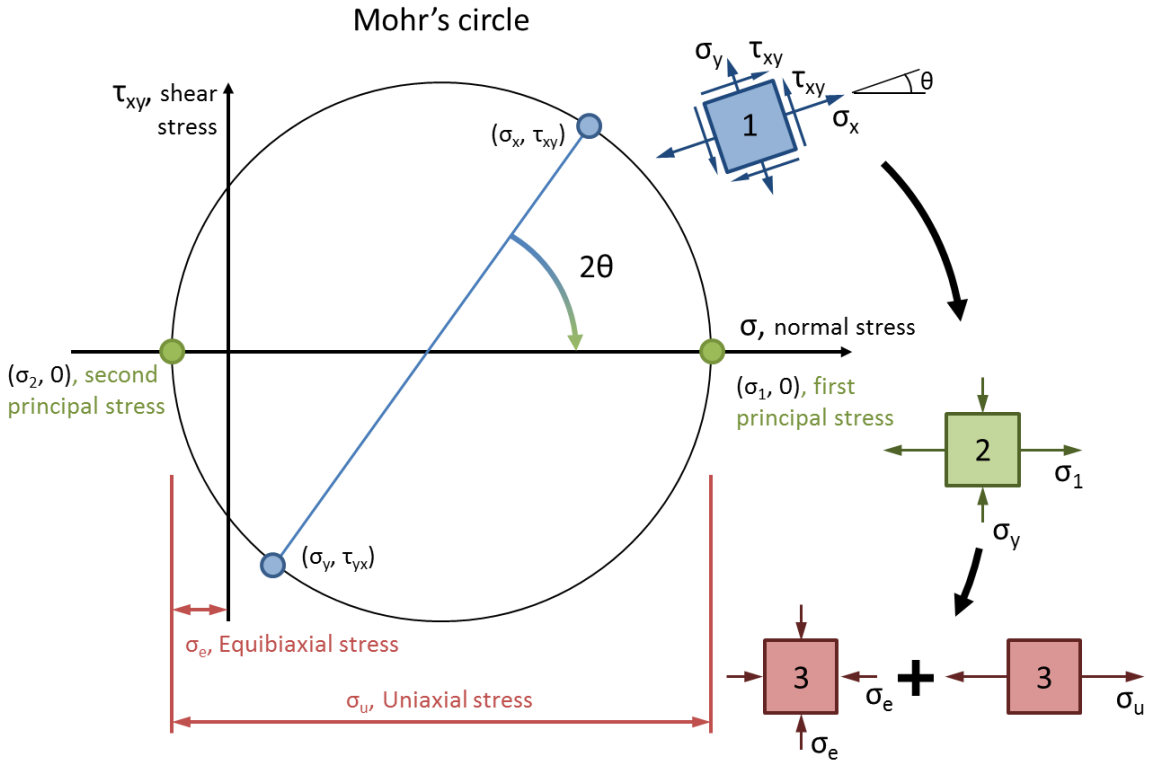

Figure 9. Mohr's circle, illustrating the different representations of stress used in this work

3.3 Physics of stress generation

The stress-fluence curve of the materials discussed here results from three primary mechanisms: morphology changes, relaxation, and thermal-spike driven stress generation. These three mechanisms have been studied in detail by other researchers, and models have been developed to describe the behavior of some materials[18,19,20]. Here we briefly describe these mechanisms.

Crystalline silicon and glasses undergo changes in morphology, which results in a density change. Crystalline silicon becomes amorphous as it is damaged from implantation[19]. Since amorphous silicon is less dense than crystalline silicon, the expansion results in a compressive stress in the implanted region. This is believed to be the primary mechanism driving compressive stress in silicon. In contrast, silicate glasses typically exhibit an increase in density, and therefore a tensile stress, due to morphology changes[21]. Density changes result in an isotropic strain, and therefore an equi-biaxial stress. While Eagle XG experiences this densification, it appears that Schott D-263 exhibits very little densification. Since a densification results in a tensile stress, most glasses show an initial increase in tensile stress. Figure 7 illustrates that Schott D-263, especially for high ion energy, does not exhibit this behavior nearly to the same degree as typical glasses: the stress is compressive almost immediately after the ion beam impinges on the sample.

Beyond morphology changes, amorphous materials experience stress generation and relaxation, which appear to be due to the same phenomena: thermal spikes caused by very large energy deposition density from an incoming ion. For high-energy light ions, such as 6 MeV Si^{+++}, the vast majority of energy transfer between the ion and substrate is via the electronic subsystem, rather than nuclear collisions. This energy transfer is confined to a long, narrow cylinder several microns long and only a few nanometers in diameter. A simple model describing the strain resulting from this thermal spike is described by Trinkaus and Ryazanov[20]. An illustration of the following process is shown in Figure 10. First, rapid heating in the ion track causes thermal expansion relative to the substrate. Due to the large aspect ratio (length/diameter ~ 1000) of the ion track, significant deviatoric stress (i.e., non-pressure stress) develops in the ion track. Next, this deviatoric stress relaxes due to reduced viscosity of the heated amorphous material, leaving only pressure in the ion track. Finally, upon cooling, the residual stress in the ion track is compressive perpendicular to the ion track axis, and tensile along the axis. Many randomly-located thermal spikes result in an average stress build-up throughout the implanted layer.

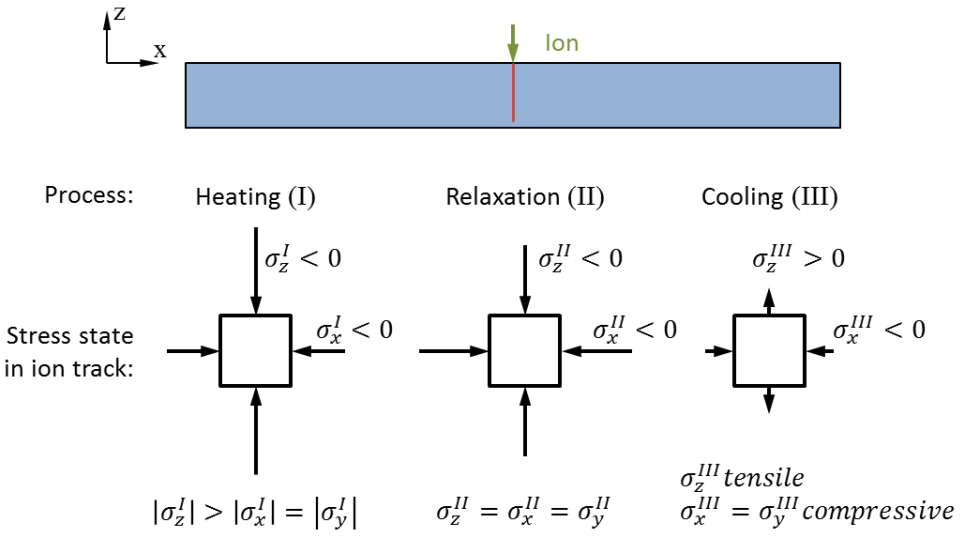

Figure 10. Illustration of thermal spike mechanism showing stress along and perpendicular to the ion track during each of the three regimes of the thermal spike stress generation process.

The relaxation mechanism is somewhat simpler. If there is some local stress in the implanted layer before a thermal spike occurs, any *deviatoric* components of that stress may relax once the ion track viscosity is low. Therefore, there are thermal spike stress generation and relaxation mechanisms that act simultaneously, and the stress in the implanted layer eventually reaches an equilibrium. As the ion beam is tilted, the tensile stress along the ion beam acts partly in-plane, and the in-plane stresses in the implanted layer may be different parallel to and perpendicular to the projection of the ion beam vector onto the substrate surface. This explains the results shown in Figure 8.

4. MONTE CARLO SIMULATIONS

4.1 Simulated correction of conical shell mirrors

Since we have shown that we can control the full plane stress tensor of Schott D-263 glass, we would like to know what level of residual figure error could be corrected using ion implantation. To do this, we use an algorithm as described in Section 3.2 for a general surface strain field generation. That is, we impose no constraint on the magnitude of stress we can apply. Instead we simply check whether the surface is correctable given the magnitudes of stress we can generate.

Since we do not have a set of actual figure errors of D-263 mirrors, we perform a Monte Carlo simulation with fictive surfaces: we generate a number of fictive surfaces with error functions composed of Legendre-Legendre polynomials that have approximately a power-law power spectral density function and mean initial residual HPD ≈ 8 arcsecond. The slope of the PSD is -2 decades/decade, and we have included spatial wavelengths down to 4 mm, limited for now by the Finite Element mesh size. A sample set of power spectral densities, and a histogram showing the distribution of initial figure error, are shown in Figure 11. For all of the corrections, the residual surface error after correction is better than 0.05 arcsecond HPD. This small residual may be due to approximations made to speed the calculation. Figure 12 shows the fraction of mirrors that could be fully corrected (to 0.05 arc-sec HPD or better) in each bin, based on our experimental results with uni-axial and equi-biaxial stress. We made no effort to find a best correction for the samples that were not correctable. We found that almost all large-radius mirrors (R ≥ 500 mm) we tested were fully correctable. It is again clear that mirrors with a smaller radius are more difficult to correct.

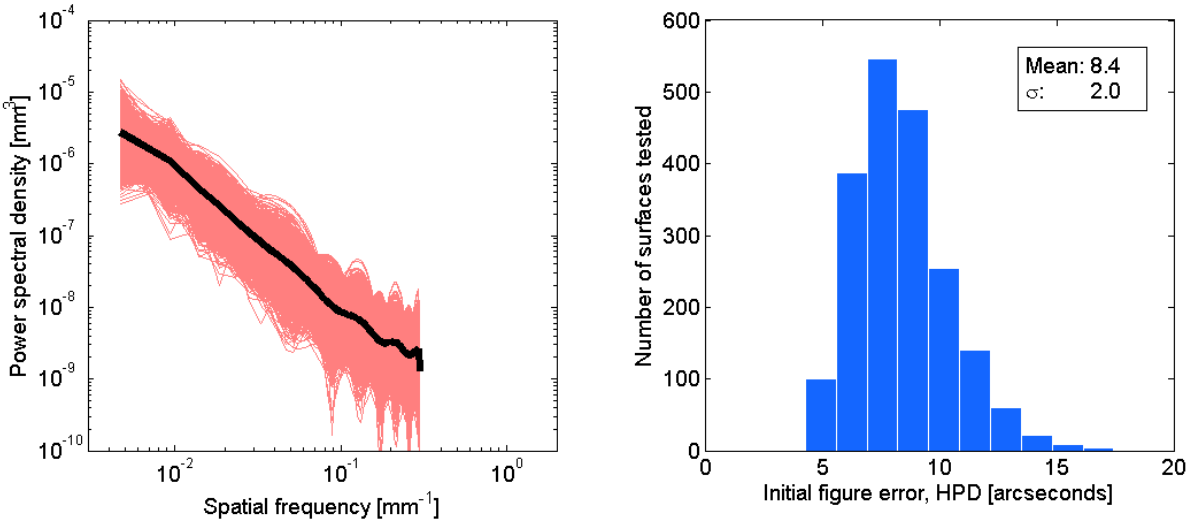

Figure 11. Figure errors of mirrors corrected in Monte Carlo simulation. Left: Power spectral density (black line is the average PSD). Right: histogram of initial figure errors.

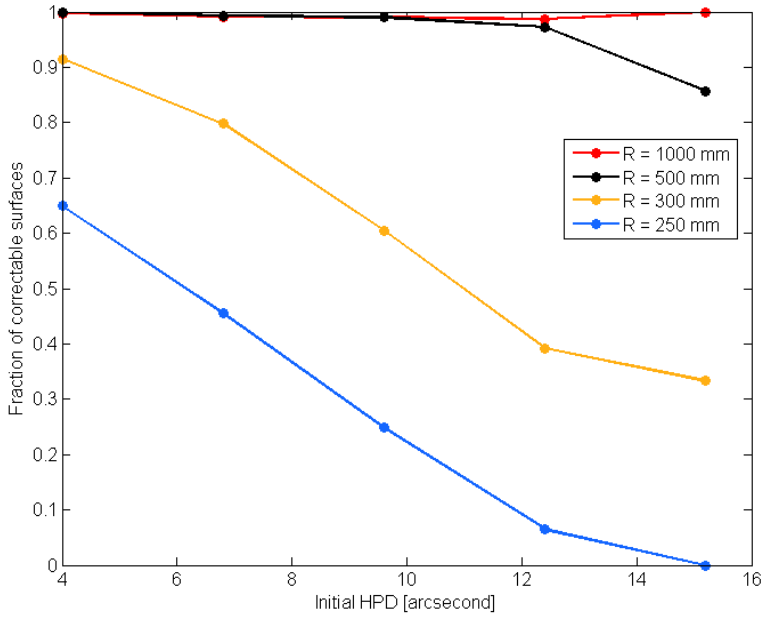

Figure 12. Almost all large-radius mirrors could be fully corrected. The fraction of correctable surfaces decreases rapidly with decreasing radius of curvature, and with increasing initial error.

4.2 Sensitivity of correction to stress errors

We conducted a simple Monte Carlo simulation to estimate how sensitive the corrections are to random error in the generated stress. To do this, we randomly vary the stress at each node in the finite element model, following a normal distribution with a standard deviation equal to the error fraction we would like to test. We test error fraction standard deviations ranging from 0.1% to 10%. The results are shown in Figure 13, for such a sensitivity test for a surface with a PSD near the mean in Figure 11, and with an initial figure of 8.9 arcsecond HPD.

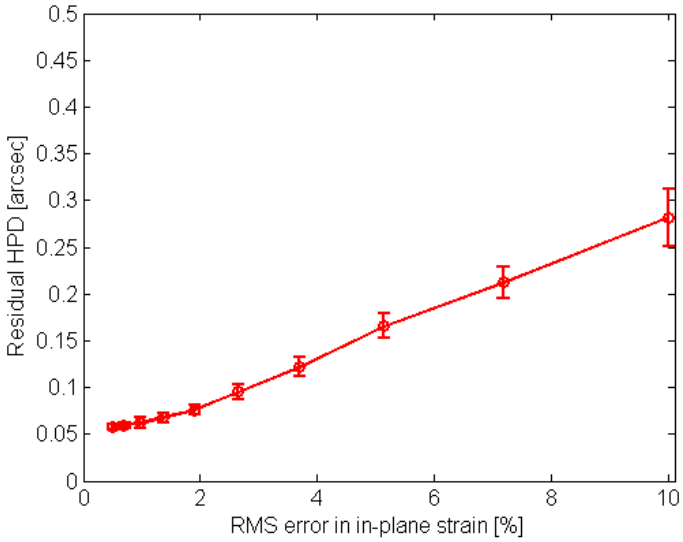

Figure 13. The residual error rises almost linearly with RMS stress magnitude error

The error bars represent the standard deviation of the results. It is evident from these results that we should keep the accuracy of stress to better than about ±5% standard deviation in order to make a correction to 0.2 arcsecond HPD. However, if we allow for iterative corrections, we could relax this requirement. This analysis is also of course only valid for a specific surface; before specifying accuracy requirements we will need to evaluate real surfaces.

5. FUTURE WORK

We are currently in the process of building a vacuum chamber with the ability to manipulate large substrates (200 mm x 130 mm) in two rotational degrees of freedom. We are also extending the accelerator beam-line we currently use to allow expanded ion beam scanning capability, to cover these large substrates. We expect this new hardware to allow us to correct figure errors in flat and curved mirror substrates, and to gain a better understanding of ion implantation. A representative diagram of this chamber is shown in Figure 14. The mechanical components have been removed for clarity.

Previously, we have shown stress stability results for implanted samples[14,16], as well as results showing no roughening of implanted substrates. These are very important aspects to consider, and could impact the usefulness of ion implantation substantially. Those experiments were conducted on samples implanted with much lower ion beam energy than we currently use, so we plan to repeat these experiments with the current implant parameters.

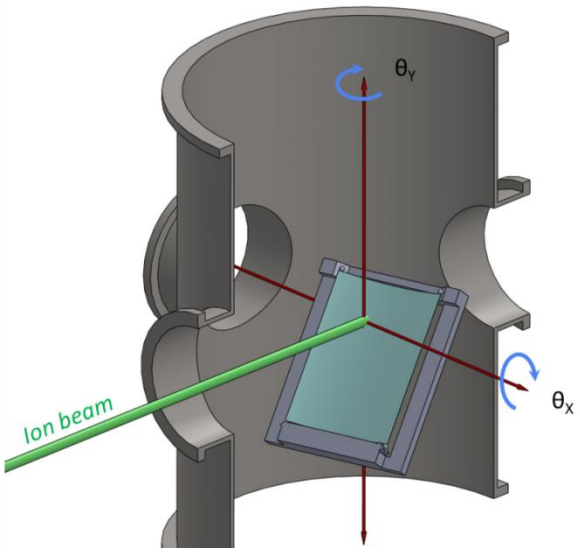

Figure 14. CAD image of mechanical components of vacuum chamber currently being built

6. CONCLUSIONS

We have shown that with ion implantation we can generate substantial equi-biaxial stress in Schott D-263 glass, Corning Eagle XG glass, and crystalline silicon substrates; and we can additionally control the direction of stress in Schott D-263 glass. With this ability in Schott D-263, in theory we may provide a nearly-full correction, to about 0.01 arcsecond RMS axial slope error, over the entire surface. This requires no external loads via the mounting structure.

ACKNOWLEDGEMENTS

The authors would like to thank Will Zhang, Jay Fucetola, Heng Zuo, Michael DeTienne, and Alex Bruccoleri for helpful discussions. This work has been financially supported by the NASA APRA grant NNX14AE76G, the MIT Kavli Institute Research Investment Fund, and the National Science Foundation Graduate Research Fellowship Program.

REFERENCES

[1] M. C. Weisskopf, J. Gaskin, H. Tananbaum, and A. Vikhlinin, "Beyond Chandra: the x-ray Surveyor," in *Proceedings of SPIE*, 2015, vol. 9510, p. 951002.

[2] W. W. Zhang, M. P. Biskach, V. T. Bly, J. M. Carter, K. W. Chan, J. A. Gaskin, M. Hong, B. R. Hohl, W. D. Jones, J. J. Kolodziejczak, L. D. Kolos, J. R. Mazzarella, R. S. McClelland, K. P. McKeon, T. M. Miller, S. L. O'Dell, R. E. Riveros, T. T. Saha, M. J. Schofield, M. V. Sharpe, and H. C. Smith, "Affordable and lightweight high-resolution x-ray optics for astronomical missions," in *Proceedings of SPIE*, 2014, vol. 9144, p. 914415.

[3] E. Sung, B. Chalifoux, M. L. Schattenburg, and R. K. Heilmann, "Non-touch thermal air-bearing shaping of x-ray telescope optics," in *Proceedings of SPIE*, 2013, vol. 8861, p. 88610R.

[4] A. Winter, E. Breunig, P. Friedrich, and L. Proserpio, "Progress on indirect glass slumping for future x-ray telescope optics," in *Proceedings of SPIE*, 2014, vol. 9144, p. 91441C.

[5] W. W. Zhang, M. P. Biskach, P. N. Blake, V. T. Bly, J. M. Carter, K. W. Chan, J. A. Gaskin, M. Hong, B. R. Hohl, W. D. Jones, J. J. Kolodziejczak, L. D. Kolos, J. R. Mazzarella, R. S. McClelland, K. P. McKeon, T. M. Miller, S. L. O'Dell, R. E. Riveros, T. T. Saha, M. J. Schofield, M. V. Sharpe, and H. C. Smith, "High resolution and high throughput x-ray optics for future astronomical missions," in *Proceedings of SPIE*, 2013, vol. 8861, p. 88610N.

[6] K. Kilaru, B. D. Ramsey, M. V. Gubarev, J. A. Gaskin, S. L. O'dell, and W. Zhang, "Differential deposition to correct surface figure deviations in astronomical grazing-incidence x-ray optics," in *Proceedings of SPIE*, 2011, vol. 8147, p. 81470X.

[7] P. B. Reid, T. L. Aldcroft, R. Allured, V. Cotroneo, R. L. Johnson-Wilke, V. Marquez, S. McMuldroch, S. L. O'Dell, B. D. Ramsey, D. A. Schwartz, S. E. Trolier-McKinstry, A. A. Vikhlinin, R. H. T. Wilke, and R. Zhao, "Development status of adjustable grazing incidence optics for 0.5 arcsecond x-ray imaging," in *Proceedings of SPIE*, 2014, vol. 9208, p. 920807.

[8] M. P. Ulmer, X. Wang, J. Cao, J. Savoie, B. Bellavia, M. E. Graham, and S. Vaynman, "Progress report on using magneto-strictive sputtered thin films to modify the shape of a x-ray telescope mirror," in *Proceedings of SPIE*, 2012, vol. 8503, p. 85030C.

[9] S. L. O'Dell, T. L. Aldcroft, R. Allured, C. Atkins, D. N. Burrows, J. Cao, B. D. Chalifoux, K.-W. Chan, V. Cotroneo, R. F. Elsner, M. E. Graham, M. V. Gubarev, R. K. Heilmann, R. L. Johnson-Wilke, K. Kilaru, J. J. Kolodziejczak, C. F. Lillie, S. McMuldroch, B. D. Ramsey, P. B. Reid, R. E. Riveros, J. M. Roche, T. T. Saha, M. L. Schattenburg, D. A. Schwartz, S. E. Trolier-McKinstry, M. P. Ulmer, S. Vaynman, A. Vikhlinin, X. Wang, M. C. Weisskopf, R. H. T. Wilke, and W. W. Zhang, "Toward large-area sub-arcsecond x-ray telescopes," 2014, vol. 9208, pp. 920805.

[10] J. J. Kolodziejczak, C. Atkins, J. M. Roche, S. L. O'Dell, B. D. Ramsey, R. F. Elsner, M. C. Weisskopf, and M. V. Gubarev, "Active figure control effects on mounting strategy for x-ray optics," in *Proceedings of SPIE*, 2014, vol. 9208.

[11] T. L. Aldcroft, D. A. Schwartz, P. B. Reid, V. Cotroneo, and W. N. Davis, "Simulating correction of adjustable optics for an x-ray telescope," in *Proceedings of SPIE*, 2012, vol. 8503, p. 85030F.

[12] R. S. McClelland, M. P. Biskach, K.-W. Chan, R. A. Espina, B. R. Hohl, T. T. Saha, and W. W. Zhang, "Process of constructing a lightweight x-ray flight mirror assembly," in *Proceedings of SPIE*, 2014, vol. 9144, p. 914441.

[13] Y. Huang, D. Ngo, X. Feng, and A. J. Rosakis, "Anisotropic, non-uniform misfit strain in a thin film bonded on a plate substrate," *Interact. Multiscale Mech.*, vol. 1, no. 1, pp. 123–142, 2007.

[14] B. D. Chalifoux, "Ion implantation for figure correction of high-resolution x-ray telescope mirrors," M.S. Thesis, Massachusetts Institute of Technology, 2014.

[15] W. N. Davis, P. B. Reid, and D. A. Schwartz, “Finite element analyses of thin film active grazing incidence x-ray optics,” in *Proceedings of SPIE*, 2010, p. 78030P.
[16] B. Chalifoux, R. K. Heilmann, and M. L. Schattenburg, “Shaping of thin glass X-ray telescope mirrors using air bearing slumping and ion implantation,” in *Proceedings of SPIE*, 2014, vol. 9144, p. 91444D.
[17] S. Klaumünzer, “Ion tracks in quartz and vitreous silica,” *Nucl. Instrum. Methods Phys. Res. Sect. B Beam Interact. Mater. At.*, vol. 225, no. 1–2, pp. 136–153, Aug. 2004.
[18] E. Snoeks, T. Weber, A. Cacciato, and A. Polman, “MeV ion irradiation-induced creation and relaxation of mechanical stress in silica,” *J. Appl. Phys.*, vol. 78, no. 7, pp. 4723–4732, Oct. 1995.
[19] C. A. Volkert, “Stress and plastic flow in silicon during amorphization by ion bombardment,” *J. Appl. Phys.*, vol. 70, no. 7, pp. 3521–3527, Oct. 1991.
[20] H. Trinkaus and A. I. Ryazanov, “Viscoelastic Model for the Plastic Flow of Amorphous Solids under Energetic Ion Bombardment,” *Phys. Rev. Lett.*, vol. 74, no. 25, pp. 5072–5075, Jun. 1995.
[21] R. A. B. Devine, “Macroscopic and microscopic effects of radiation in amorphous SiO2,” *Nucl. Instrum. Methods Phys. Res. Sect. B Beam Interact. Mater. At.*, vol. 91, no. 1–4, pp. 378–390, Jun. 1994.